ACS OMEGA

Open Access

http://pubs.acs.org/journal/acsodf

Article

Green Synthesis of TiO_2 Using *Impatiens rothii* Hook.*f*. Leaf Extract for Efficient Removal of Methylene Blue Dye

Getye Behailu Yitagesu, Dereje Tsegaye Leku,* and Getachew Adam Workneh*

Cite This: *ACS Omega* 2023, 8, 43999−44012

Read Online

ACCESS | Metrics & More | Article Recommendations | Supporting Information

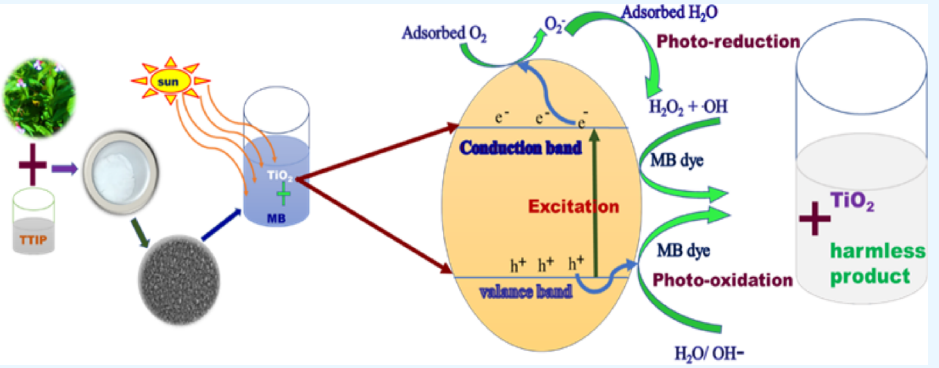

ABSTRACT: In this work, TiO_2 nanoparticles (NPs) were effectively synthesized by a green method using the *Impatiens rothii* Hook.*f*. leaf (IL) extract as a capping and reducing agent. The as-synthesized TiO_2 NPs were characterized by different characterization methods such as the Brunauer−Emmett−Teller (BET) analysis, high-resolution transmission electron microscopy (HRTEM), scanning electron microscopy (SEM), energy dispersive X-ray spectroscopy (EDX), Fourier transform infrared spectroscopy (FTIR), X-ray photoelectron spectroscopy (XPS), diffused reflectance spectroscopy (DRS), and X-ray diffraction (XRD) and Raman spectroscopy. The specific surface area from BET analysis was found to be 65 m^2/g. The average crystallite size from XRD analysis and average particle size from SEM analysis were found to be ∼11 and ∼25 nm, respectively. The Raman spectroscopy and XRD results showed that the biosynthesized (IL−TiO_2) nanoparticles were purely anatase phase. XPS analysis illustrated the formation of Titania with an oxidation state of +4. The DRS study showcased that a blue-shifted intense absorption peak of IL−TiO_2 (3.39 eV) compared to the bulk material reported in the literature (3.2 eV). HRTEM micrograph showed the presence of grain boundary with *d* spacings of 0.352, 0.245, and 0.190, which correspond to the lattice planes of (101), (004), and (200), respectively. From the EDX analysis, the weight percents of titanium and oxygen were found to be 54.33 and 45.67%, respectively. The photoinduced degradation of methylene blue (MB) dye was investigated in the presence of biosynthesized IL-TiO_2 NPs photocatalyst. The effect of parameters like catalyst dosage (30 mg/L), initial concentration of MB (15 ppm), pH (10.5), and contact time (100 min) on the removal efficiency was optimized. The maximum photodegradation efficiency under the optimized conditions was found to be 98%.

1. INTRODUCTION

The tremendous environmental effects, such as climate change, water pollution, and depletion of natural resources caused by industrialization, are linked with an increasing socio-economic demand. The natural world is being severely contaminated by the uncontrolled discharge of many hazardous substances including liquid, semisolid, and solid wastes.[1,2] Nowadays, one of our world challenges is the opportunity to get pure water due to pollution. Among the causes of water contamination include energy byproducts, mining operations, insect sides and chemical fertilizers, radioactive wastes, infrastructural activities, and industrial effluents including dyes.[3] Numerous sectors, including those in the leather, textile, printing, cosmetics, and pharmaceuticals, release synthetic dyes, which are significant sources of water pollution.[4] One toxic and nonbiodegradable organic chemical that is frequently utilized in the textile industries is methylene blue (MB). Additionally, due to its planar shape, it is very soluble in water.[5] Therefore, the reprocessing and treatment of wastewater is the primary activity to reduce environmental pollution and avoid the shortage of a clean water supply.

Received: August 19, 2023
Revised: October 16, 2023
Accepted: October 26, 2023
Published: November 10, 2023

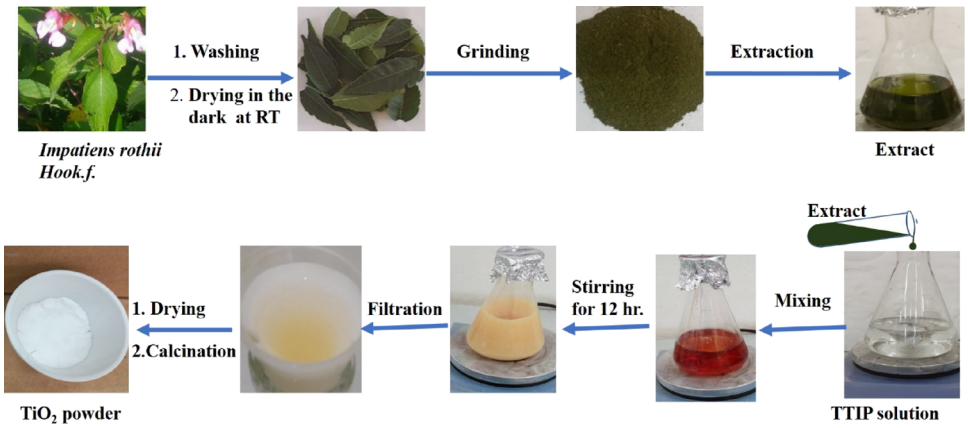

Figure 1. Schematic representation of plant leaf extraction and green synthesis of TiO_2. Photograph courtesy of "Getye Behailu Yitagesu". Copyright 2023.

There are a number of wastewater treatment methodologies whose primary objective is to reduce pollutants. These include physicochemical methods, electrochemical oxidation, biological processes, adsorption processes, and advanced oxidation processes (like photocatalysis).[6−10] Among the methods mentioned, photocatalytic degradation is thought to be the most promising because it is simple to use, quick, clean, and inexpensive compared to other methods, which have high operating costs and take a long time to remove organic contaminants from water.[11] Photocatalysis is the utilization of photon energy to initiate a given reaction process. Due to their capacities to destroy different organic contaminants found in water through a series of redox processes, semiconductor materials have drawn increased attention in the field of photocatalysis. The photocatalytic ability of semiconductors is related to the excitation of electrons from the valence band to the conduction band caused by the absorption of a photon with an appropriate wavelength.

There are four basic steps in the photocatalysis of pollutants: (1) absorption of light having an energy greater than the band gap of semiconductor material to form electron−hole pairs (excitons), (2) separation of excitons, (3) migration of electrons and holes to the surface of the semiconductor, and (4) the charged electrons and holes participating in the redox processes (electrons are utilized in reduction, and holes are utilized in oxidation process).[12−14] In recent decades, transition metal oxides such as ZrO_2,[15] CuO,[16] WO_3,[17] ZnO,[18] and TiO_2[19] are the well-known photocatalysts that generate the redox reactions at their surfaces when stimulated by the UV−visible light irradiation appropriate to their band gap energy.[12,20,21] Among them, TiO_2 is the most effective in photocatalytic splitting of water and photodegradation of organic pollutants and has good antibacterial activity.[22]

Due to its numerous benefits, such as great photocatalytic ability, high oxidizing power, low toxicity and biocompatibility, excellent chemical stability, and ease of accessibility, TiO_2 is one of the best materials for photocatalytic processes.[21,23] There are three crystallographic forms of TiO_2, namely, anatase (tetragonal), rutile (tetragonal), and brookite (orthorhombic).[24,25] In general, TiO_2 is considered as an ecologically friendly and has been used in various industrial applications including gas sensors,[26] corrosion protection,[27] white pigment,[28] dye-sensitized solar cells,[29] remediation of the environment,[30] hydrogen gas production,[31] providing high dielectric constant and high electrical resistance,[32] and reduction of carbon dioxide.[33]

Titanium dioxide NPs can be synthesized using a variety of methods, including sol−gel, sono-chemical, microwave-assisted,[34] deposition, hydro/solvothermal, and oxidation methods.[30,35] Biosynthesis of titanium dioxide NPs has gained wide attention among scholars due to its cost-effective, eco-friendly, and reproducible method.[25] The green synthesis method of nanoparticles with the help of plants has many benefits, one of which is the elimination of the need for chemical stabilizing agents.[36] Plant extracts can act as both reducing agents and stabilizers at the same time, and such a method also reduces the use of various chemical substances and makes use of natural substances, which further lowers the toxicity level of TiO_2 nanoparticles.[37,38]

In the present study, we have successfully synthesized TiO_2 NPs using *Impatiens rothii* Hook.*f.* leaf as a capping and reducing agent. *Impatiens rothii* Hook.*f.* is a flora classified under the family of Balsaminaceae.[39] It is a tuberous species native to Ethiopia and used as local wound treatment, especially for fire burn skin. In addition to this, its root extract is used for nails and palm adornment due to its colorfulness and high adhesive property. To the best of our knowledge, this plant is not used for the synthesis of TiO_2 nanomaterials. The resulting biosynthesized TiO_2 nanoparticles are not also tested for photocatalytic degradation of potential pollutant methylene blue (MB). The biosynthesized IL-TiO_2 showed good mesoporous behavior with a surface area of 56 m^2/g. The SEM morphology also revealed almost uniform NPs with less agglomeration, which can be attributed to the capping ability of *Impatiens rothii* Hook.f. leaf extract during synthesis. Therefore, this mesoporous structure can contribute to enhancing the photocatalytic activity of IL-TiO_2 against the MB dye.

2. EXPERIMENTAL SECTION

2.1. Materials and Chemicals. The materials used in this work were titanium tetra isoprpoxide (TTIP, 97.5%, Merck, Germany), ethanol (99.9%, Luba, India), ascorbic acid ($C_6H_8O_6$) (SRL, 99%), deionized water, sodium hydroxide (98%, Luba, India), methylene blue ($C_{16}H_{18}ClN_3S$, Dallul Pharmaceuticals plc), and *Impatiens rothii* Hook.f. plant leaf

2.2. Extraction of Plant Leaves. The extraction was done following the method reported by Basit and colleagues with modification.[40] The fresh leaves of *Impatiens rothii* Hook.f.

https://doi.org/10.1021/acsomega.3c06142
ACS Omega 2023, 8, 43999−44012

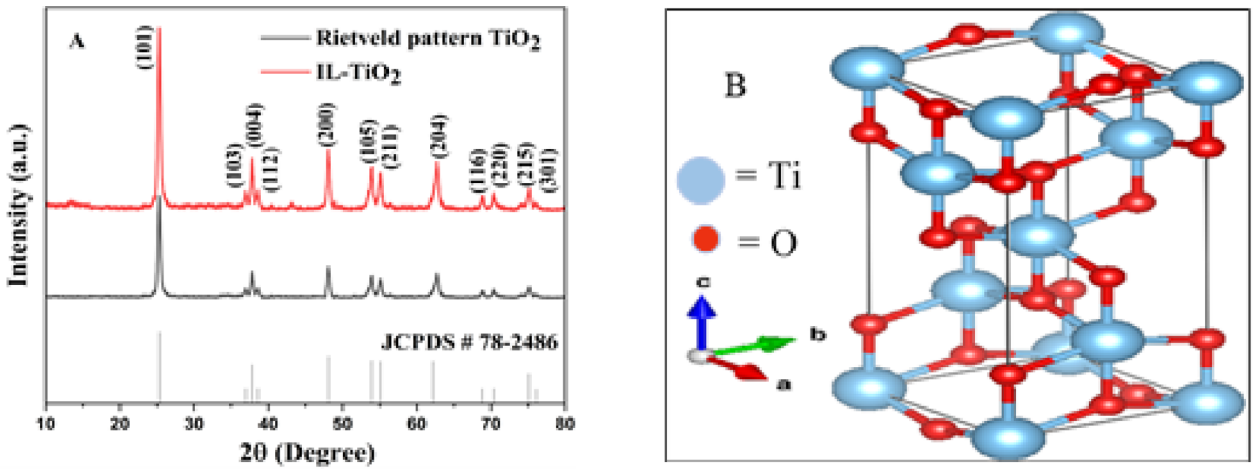

Figure 2. X-ray diffraction (A); 3D VESTA visualization (B) of IL−TiO_2 NPs.

were collected from Menz Gera Midir, Amhara regional state, Ethiopia. The collected leaves undergo washing with deionized water to remove dust and suspended particles. Then, the leaves were dried in the dark at room temperature (RT) for 2 weeks. The dried leaves were ground with a mortar and pestle. An amount of 20 g of leaves powder was taken into 500 mL of deionized water and boiled at 60 °C for 4 h through stirring magnetically at stirring speed of 600 rpm. The resulting extracted solution was allowed to cool and was filtered by using Whatman filter paper No. 1. The filtrate was used to synthesize TiO_2 nanoparticles as shown in Figure 1.

2.3. Synthesis of TiO_2 Nanoparticles. An amount of 15 mL of titanium tetra isopropoxide (TTIP) was dissolved in 50 mL ethanol. Then, 50 mL of the plant extract solution was added to the precursor solution slowly with vigorous stirring for 12 h until yellowish-colored precipitate formed (Figure 1). After standing for a night (12 h), the precipitate was filtered by Whatman filter paper no. 1 followed by washing 3 times with deionized water and twice with ethanol. Next to filtration, the paste was dried at 80 °C for 3 h in a hot air oven. The dried powder was ground using mortar and pestle and calcined at 500 °C for 3 h in a muffle furnace with a heating rate of 10 °C/min.

2.4. Characterization of the As-Synthesized TiO_2 NPs. The characteristics of IL−TiO_2 NPs were studied by using various techniques. The thermogravimetric analysis/differential thermal analysis (TGA/DTA) curve was obtained on thermal analyzer (DTG-60H Shimadzu Co., South Korea) instrument in a temperature range of 0 to 800 °C at a heating rate of 10 °C/min. The X-ray diffraction (XRD) analysis was carried out using a Shimadzu 7000 X-ray diffractometer (Japan) equipped with Cu Kα1 radiation source (λ = 1.5406 Å) with an accelerating voltage of 40 kV and a source current of 30 mA at a scanning rate of 4° min^{-1} in a 2θ range of 10 to 80°. BET analysis of pore size, pore volume, and specific surface area distribution was evaluated by measuring nitrogen adsorption−desorption at 77.7 K using a Quantachrome v11.02, USA, instrument.

The Raman spectrum was analyzed by a Raman spectrophotometer (JASCO, NRS-5000, Japan). X-ray photoelectron spectroscopy (XPS) was measured by a Kratos Axis DLD X-ray photoelectron spectrometer (Shimadzu, Canada). The UV−vis DRS and dye absorbance were recorded on a UV−vis defused reflectance spectrophotometer (JASCO V-750 UV−vis). FTIR spectra were recorded in the range of 4000 to 400 cm^{-1} on an FTIR-6600 spectrophotometer (JACO International Co., Ltd., Tokyo, Japan). The morphology of IL-TiO_2 NPs was studied by the SEM technique (400, FEG, USA). Energy-dispersive spectroscopy attached to SEM was used to analyze the elemental composition. High-resolution lattice images were achieved by means of a transmission electron microscope with an operating voltage of 300 kV (FEI, Titan, 80−300 kV).

2.5. Photocatalytic Performance Test. The photocatalytic degradation activity of IL−TiO_2 NPs against methylene blue dye was tested under a 150 W tungsten-halogen lamp (Philips, China). An amount of 60 mL of aqueous solution of MB (5−20 ppm) was prepared in vessels, and an appropriate amount of IL−TiO_2 NPs (10−50 mg) was added. The solutions were sonicated in dark for 10 min and allowed to stand for 30 min prior to irradiation for adequate adsorption−desorption equilibrium. In every 10 min interval, 4 mL of MB solution was taken from the reaction mixture and absorbance was measured by a UV−vis spectrophotometer. To study the effect of pH on the photocatalytic degradation ability of IL−TiO_2 NPs, the point of zero charge was obtained (pH_{ZPC} = 7.32) by the salt addition method (Figure S1).[41] Then, based on the pH_{ZPC} value, photocatalytic activity was done at different pH (8−11.5). The pH values were adjusted by adding 0.1 M NaOH solution. The percent removal of MB dye by IL−TiO_2 NPs was calculated using the formula in eq 1.[40]

$$\%\text{degradation} = \frac{C_0 - C}{C_0} \times 100 = \frac{A_0 - A}{A_0} \times 100 \quad (1)$$

where C_0 and A_0 are dye concentration and absorbance, respectively, before irradiation. The parameters C and A are the concentration of MB dye and its absorbance, respectively, at any time after the irradiation has started. The pseudo first order kinetic model in eq 2 was used to investigate the rate of photocatalytic degradation of MB dye.

$$\ln\left(\frac{C_0}{C}\right) = kt \quad (2)$$

where C_0 and C are initial concentrations of MB dye at the start of catalysis and after a given time t, respectively. The rate constant k is obtained from the slope of the curve ln(Co/C) against t.[42,43]

https://doi.org/10.1021/acsomega.3c06142
ACS Omega 2023, 8, 43999−44012

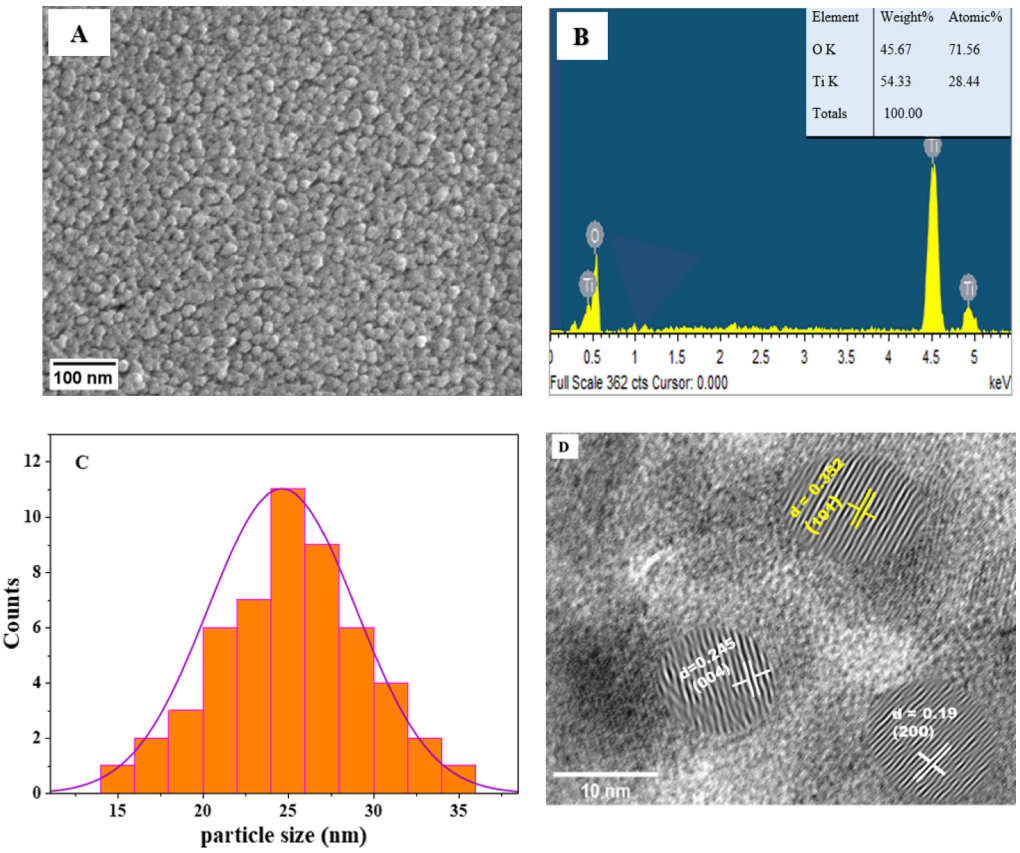

Figure 3. SEM micrograph (A), EDX (B), particle size histogram from SEM (C) and HRTEM micrograph (D) of IL−TiO_2.

2.6. Reusability Test. The recyclability tests were done for IL−TiO_2 after being used in the photocatalytic degradation of MB. After the first photocatalysis degradation, the solution was centrifuged three times with distilled water. Then, the washed IL−TiO_2 was dried at 70 °C and reused. This procedure was repeated for four consecutive additional cycles of photocatalysis using fresh MB dye.

3. RESULTS AND DISCUSSION

3.1. Characterization. *3.1.1. TGA Analysis.* The thermal decomposition property of IL−TiO_2 NPs was evaluated between room temperature and 800 °C. Figure S2 demonstrates thermal differential analysis (DTA) coupled with thermogravimetric analysis (TGA). The TGA curve shows three main steps of mass loss. The first nearly 6% weight loss between 36 and 150 °C represented the loss of adsorbed water. The second approximately 4% mass loss that observed between 180 and 420 °C could be attributed to the volatilization of organic matters from TTIP precursor, the transformation of amorphous structure to a crystalline form, and the elimination of chemisorbed hydroxyl groups. The third weight loss in the temperature range of 580−610 °C and exothermic peaks at 590 °C can be attributed to the phase transformation of anatase to rutile polymorph.[44]

3.1.2. XRD Analysis. The XRD pattern of IL-TiO_2 NPs was investigated with the Rietveld profile matching method with the help of Xpert High Score plus software. The Rietveld pattern fitting of IL−TiO_2 NPs' XRD, as shown in Figure 2A, demonstrates the high quality of fitting within space group of I41/amd anatase. The peaks obtained at 2θ values of 25.32, 37.07, 37.99, 38.58, 48.12, 53.97, 55.16, 62.79, 68.87, 70.42, 75.07, and 76.14° are indexed to crystal planes of (101), (103), (004), (112), (200), (105), (211), (204), (116), (220), (215), and (301), respectively, with a JCDPS card number of 78−2486.[45] The tetragonal crystal structure of the anatase phase with lattice parameters $a = b = 3.786$ Å and $c = 9.517$ Å and $\alpha = \beta = \gamma = 90°$ was visualized using VESTA (Visualization for Electronic Structural Analysis) win64 software (Figure 2B). The XRD profiles of the IL−TiO_2 NPs showed no signs of phase impurity. Using the Scherrer formula (eq 3), the average crystallite size of IL−TiO_2 NPs was calculated from the broadening of the peaks.[46] The calculated average crystallite size of IL-TiO_2 nanoparticles was 11 nm.

$$D = \frac{k\lambda}{\beta\cos\theta} \tag{3}$$

where D represents the average crystalline size; K is Scherrer's shape factor (0.94); λ is the wavelength of the source X-ray (0.15406 nm); β is the full width at half-maxima; and θ is Bragg's X-ray diffraction angle.

3.1.3. SEM-EDX and HRTEM Analysis. SEM analysis was used to determine the morphology of IL−TiO_2 NPs. The obtained results as shown in Figure 3A reveal that the IL−TiO_2 nanoparticles were in spherical structure and the average size was evaluated. Figure 3C showed the nanoparticle distribution, and it can be observed that particle size ranges from 15 to 35 nm with an average diameter of approximately 25 nm. The average particle size obtained from the SEM analysis is greater than the average crystallite size calculated using the Scherrer formula (eq 3) because the particle may contain two or more grains attached together due to agglomeration and aggregation effect. The elemental compo-

https://doi.org/10.1021/acsomega.3c06142
ACS Omega 2023, 8, 43999−44012

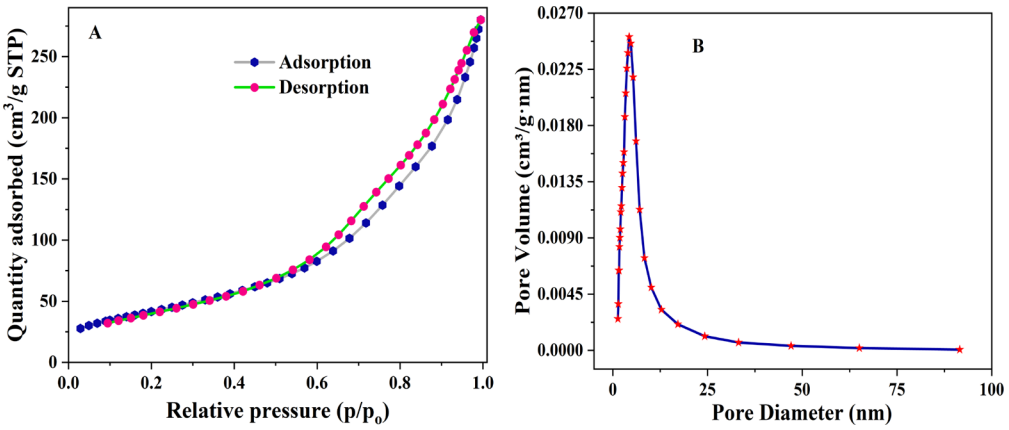

Figure 4. Nitrogen adsorption desorption isotherms (A), pore size distribution curve (B) of IL−TiO_2 NPs.

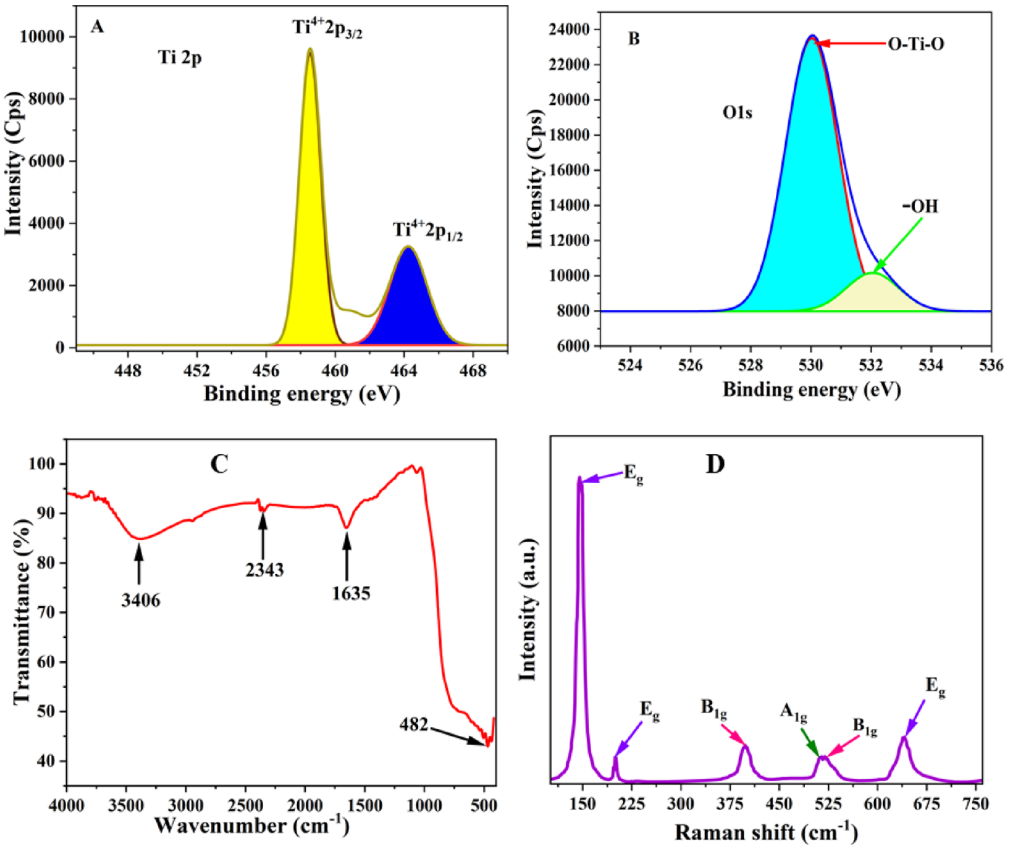

Figure 5. Deconvoluted Ti 2p XPS spectra (A) and O 1s spectra (B). FTIR spectra (C), and Raman spectra of IL-TiO_2 (D).

sition analysis of IL−TiO_2 NPs was performed by EDX analysis. As presented in Figure 3B, the weight percents of titanium and oxygen were found to be 54.33 and 45.67%, respectively, which confirms the presence of pure TiO_2 nanoparticles.

Figure 3D reveals the HRTEM micrograph of IL−TiO_2 nanoparticles. The parallel lattice fringes of the nanoparticles are clearly visible, confirming their single-crystallinity. The lattice fringes spacing 0.352, 0.245, and 0.19 nm are consistent with the (101), (004), and (200) planes of tetragonal anatase, respectively.

3.1.4. BET Study. The Brunauer−Emmett−Teller (BET) surface area analyzer was used for the surface area analysis of the as-synthesized TiO_2 NPs. In Figure 4A, a typical plot of the N_2 adsorption−desorption isotherm and showed a type IV with the hysteresis H_3 loops type in the relative pressure range of 0.57−0.9, which indicates that the synthesized nanoparticles were mesoporous.[47] The corresponding pore size distribution curve of IL−TiO_2 NPs is shown in Figure 4B. Barrett−Joyner−Halenda analysis revealed that the IL−TiO_2 NPs showed a high surface area of 65 m^2/g with the pore diameter and pore volume of 7.45 nm and 0.026 cm^3/g, respectively. A higher surface area provides more surface active parts for the adsorption of pollutants, resulting in a more efficient photocatalytic degradation process that occurs.[48] This BET result revealed that the IL−TiO_2 NPs were promising for the photocatalytic degradation of the MB dye.

https://doi.org/10.1021/acsomega.3c06142
ACS Omega 2023, 8, 43999−44012

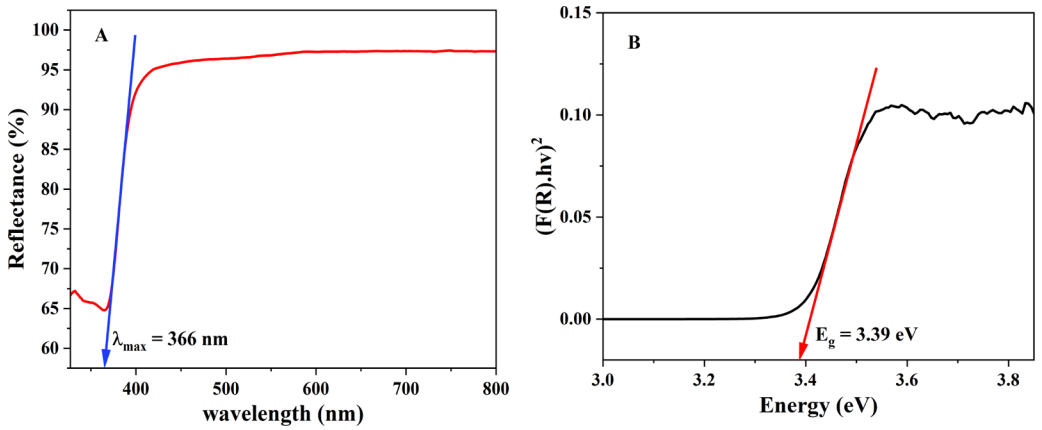

Figure 6. UV−vis DRS spectra (A); Tauc plot (B) of IL−TiO_2.

3.1.5. XPS Analysis. The X-ray photoelectron spectroscopy technique was used to confirm the oxidation state of the IL−TiO_2 nanoparticles. As shown Figure 5A, the binding energies at 458.66 and 464.14 eV resemble Ti $2p_{3/2}$ and Ti $2p_{1/2}$, respectively. The area ratio of $Ti^{4+}2p_{1/2}$ to $Ti^{4+}2p_{3/2}$ was 0.65 approximately. The difference in binding energy due to the spin orbit coupling, $\Delta E_b = E_b$ (464.14 eV) − E_b (458.66 eV) was 5.7 eV, which is well-matched with the reported values.[49,50] The O 1s spectra of IL−TiO_2 showed two peaks at binding energies of 530.5 eV and a minor peak at 532.014 eV (Figure 5B), which are attributed to oxygen anions (O−Ti−O) and surface hydroxyl (−OH) species, respectively.[51]

3.1.6. FTIR Spectroscopic Analysis. As shown in (Figure 5C) the FTIR spectrum of IL−TiO_2 consists of characteristic peaks of TiO_2. The broad band in the range of 3600−3200 cm^{-1} is attributed to the hydroxyl group of the water molecule's intermolecular interaction with the surface of TiO_2.[52,53] The absorption peak at 1635 cm^{-1} was ascribed to the bending mode of O−H bond adsorbed on the IL−TiO_2 NP surface. The strong absorption peak in the range of 850−420 cm^{-1} was attributed to the stretching band of the O−Ti−O bond.[54,55] The vibrational band at 2343 cm^{-1} is related to adsorption of atmospheric CO_2 on the surface of NPs.[55−58]

3.1.7. Raman Spectroscopic Studies. The Raman spectroscopy technique was used for structural identification of the IL−TiO_2 NPs. The Raman spectroscopy analysis of IL−TiO_2 (Figure 5D) showed tetragonal anatase Raman active modes of A_{1g}, $2B_{1g}$, and $3E_g$ vibrational spectrum centered at 515, 399, 519, 144, 197, and 639 cm^{-1}.[59−63]

3.1.8. Optical Band Gap Analysis. The Tauc plot method was used to determine the band gap energy of IL−TiO_2 based on the expression in eq 4.[64]

$$(F(R) \times h\nu)^{\frac{1}{n}} = A(h\nu - E_g) \quad (4)$$

$F(R)$ is the Kubelka−Munk function expressed in eq 5; h is Plank's constant; ν is the frequency of photon energy; the exponent n depends on the type of the electron transition; n = 1/2 for direct and n= 2 for indirect transition band gaps. A is a constant; E_g is the band gap energy.

$$F(R) = \frac{K}{S} = \frac{(1-R)^2}{2R} \quad (5)$$

where R, K, and S are the reflectance, absorption coefficient, and scattering coefficient, respectively.

The UV−visible diffused reflectance spectrum of IL−TiO_2 is shown in Figure 6A. The IL−TiO_2 showed an intense absorption peak at a wavelength of 366 nm. When compared to the bulk material of titanium oxide, the biosynthesized TiO_2 showed a blue shift. This shift in wavelength was attributed to the decrease in size of nanoparticles.[65]

Figure 6B displays the Tauc plot of IL−TiO_2. The band gap energy was estimated from the intersection point of energy-axis with the Tauc plot's linear portion. The band gap energy value was estimated to be 3.39 eV. The band gap energy of IL−TiO_2 exceeded by about 0.19 eV than that of the bulk one (3.2 eV)[19] due to the size reduction in the IL−TiO_2 nanoparticles.

3.2. Photocatalytic Performance Test. The photocatalytic degradation efficiency of IL−TiO_2 was evaluated against the methylene blue dye. The effect of parameters like catalyst dose, initial dye concentration, initial pH of dye solution, and contact time were evaluated and optimized.

3.3. Effect of IL-TiO_2 Dosage. In order to study the effect of loading ability on the dye degradation efficiency, different amounts of IL−TiO_2 NPs in the range of 10−50 mg were used for degrading 10 ppm of MB at pH of 9.5 with a contact time of 60 min as shown in Figure 7A−E. The percent of photodegradation of the dye was increased with increasing the dosage of TiO_2 up to 30 mg (68.89%), and after that, it became almost a constant value (Figure S3). As the amount of IL−TiO_2 increases, the total active sites on the surface of the catalyst increase up to some extent. However, increasing the amount of TiO_2 decreases the penetration of solar light as a consequence of the increase in turbidity of the solution. Hence, a higher amount of catalyst is not useful due to the aggregation of catalyst and reduction of the radiation field due to light scattering.[66] The highest rate constant for the degradation of MB with 30 mg of catalyst was found to be 0.0201 min^{-1} (Figure 7F). Therefore, all the experiments were performed with a 30 mg catalyst dose.

3.4. Effect of Initial Dye Concentration. The concentration of MB dye was varied from 5 to 20 ppm with an optimum IL−TiO_2 dose of 30 mg. Figure 8A−D clearly shows the difference in absorption peaks as a result of concentration increment. The rate of degradation of MB was evaluated when the concentration of MB dye was increased from 5 to 20 ppm with a constant catalyst dose of 30 mg/L. As shown in Figure 8F, 15 ppm of dye concentration resulted in higher rate of photodegradation with a rate constant of 0.020 min^{-1}. The percent of photodegradation at this concentration was recorded as 68%. A sudden decrease of photodegradation

https://doi.org/10.1021/acsomega.3c06142
ACS Omega 2023, 8, 43999−44012

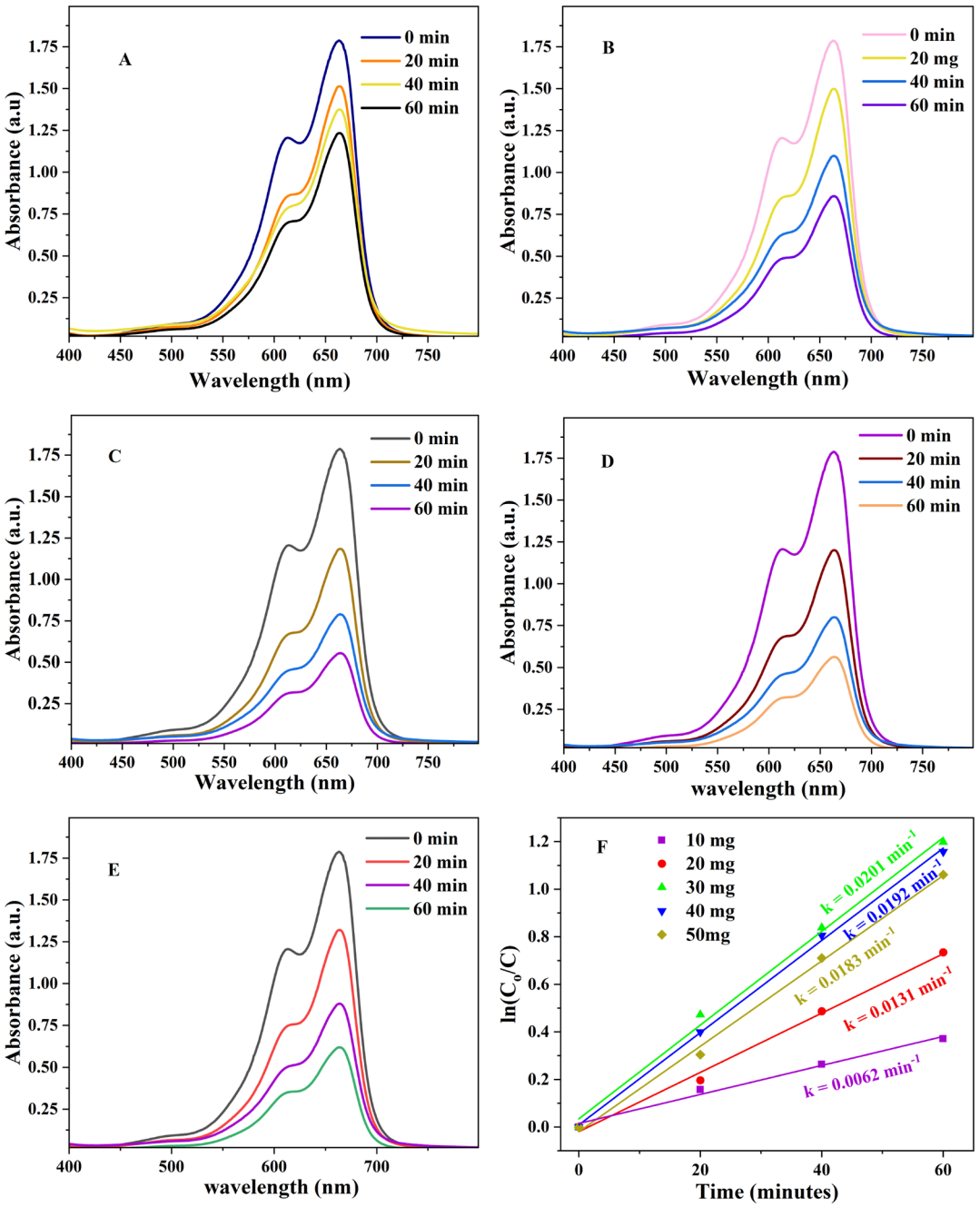

Figure 7. UV−vis absorption spectra of (A) 10, (B) 20, (C) 30, (D) 40, and (E) 50 mg of IL−TiO_2; (F) pseudo-first order model plots of (A−E).

efficiency to 45.46% (Figure 8F) as the concentration of MB dye was increased to 20 ppm was attributed to the accumulation of MB dye on the IL−TiO_2 surface that prevents the direct contact of light irradiation to the catalyst surface.[67]

3.5. Effect of Initial pH. The pH of the solution is another important factor in the photocatalytic degradation of pollutants. Photocatalyst surface charge is significantly affected by the pH of the dye solution. The pH of the MB dye solution was adjusted through adding 1 M NaOH solution. As indicated in Figure S1, the point of zero charge of IL−TiO_2 was found approximately 7.32 in which its surface is negatively charged above this point it attracts the cationic MB dye for efficient photodegradation. Then, the effect of the pH of solution on the photocatalytic degradation activity was studied within the range of 8−11.5 at optimized dye concentration (15 ppm) and photocatalyst amount (30 mg/L) as shown in Figure 9F. An increase in the photodegradation of MB dye was observed by increasing the pH of solution from 8 to 10.5 for optimized IL-TiO_2 NPs dosage as well as optimized dye concentration.

3.6. Effect of Contact Time. The rate of MB degradation on the IL-TiO_2 NP surface is equivalent to the time duration of adsorption. Figure 10A shows the contact time effect on the removal of MB at optimum conditions (30 mg of TiO_2, 15 ppm of MB, at pH 10.5) in aqueous solution. The result shows that the rapid photodegradation of methylene blue (MB) was observed in the first 80 min. As shown in Figure 10B, the removal efficiency of MB using the IL-TiO_2 catalyst was approximately 98% after an irradiation time duration of 100 min. It was found that as the time of light irradiation prolonged the percent photodegradation efficiency was increased and get

https://doi.org/10.1021/acsomega.3c06142
ACS Omega 2023, 8, 43999−44012

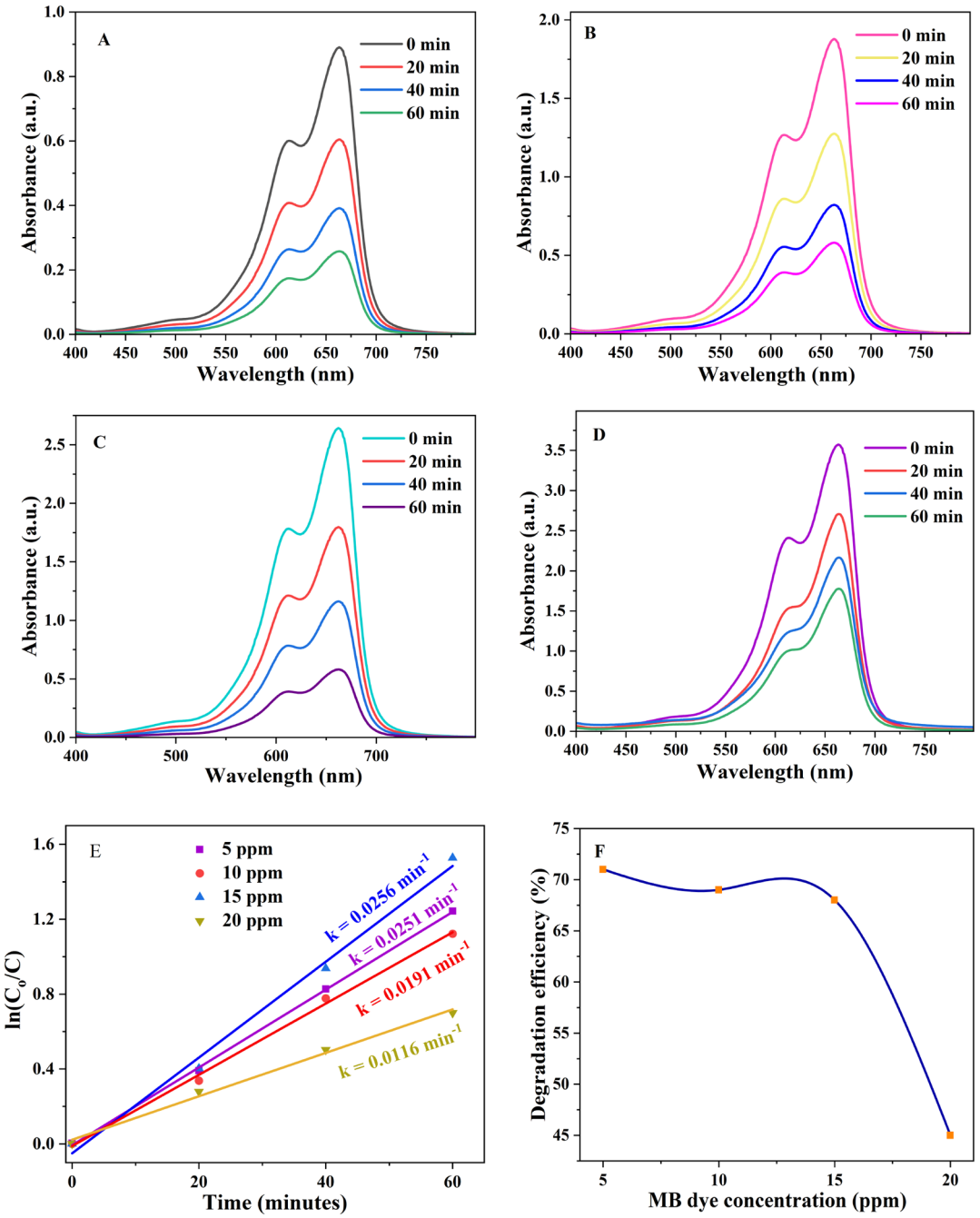

Figure 8. UV−vis absorption spectra of (A) 5, (B) 10, (C) 15, and (D) 20 ppm of MB dye; (E) pseudo-first order model plots of (A−D); (F) degradation efficiency of (A−D).

hold of a maximum after 100 min. The degradation efficiency of our work revealed good agreement with that of other works reported in Table 1.

The kinetic models of both pseudo-first (Figure 10C) and second (Figure 10D) orders were used to study the rate of photodegradation efficiency at optimized conditions. The small value of correlation coefficient (R^2 = 0.668) showed the inconsistency of the pseudo-second order kinetic model. The higher value of correlation coefficient (R^2 = 0.989) (Table 2) with a rate constant of 0.038 min^{-1} shows the good fitness of the pseudo-first order kinetic model with good photodegradation efficiency.[42,43]

3.7. Scavenging Test. The photostimulated surface properties of the as-synthesized IL-TiO_2 nanoparticles were studied for the capability of photo degradation effect on MB dye. Reactive species such as holes (h^+), superoxide radicals ($O_2^{-\bullet}$), electrons (e^-), and hydroxyl radicals ($OH^\bullet$) play a vital role in the photodegradation of organic pollutants.[74] Therefore, the photocatalytic activity of IL-TiO_2 NPs on the degradation of MB dye was studied in the presence of silver nitrate ($AgNO_3$), Ethylenediaminetetraacetic acid disodium (EDTA-2Na),[11] isopropanol (IPA),[75] and acetonitrile[76] as scavengers for e^-, h^+, $OH^\bullet$, and $O_2^{-\bullet}$, respectively, to quantify the relative contribution of reactive species. Figure 11 shows the light-assisted percent degradation of MB using IL-TiO_2 NPs in the presence of the above-mentioned radical scavengers. The scavenger tests were done using the optimum conditions. The results revealed that the hydroxyl free radicals

https://doi.org/10.1021/acsomega.3c06142
ACS Omega 2023, 8, 43999−44012

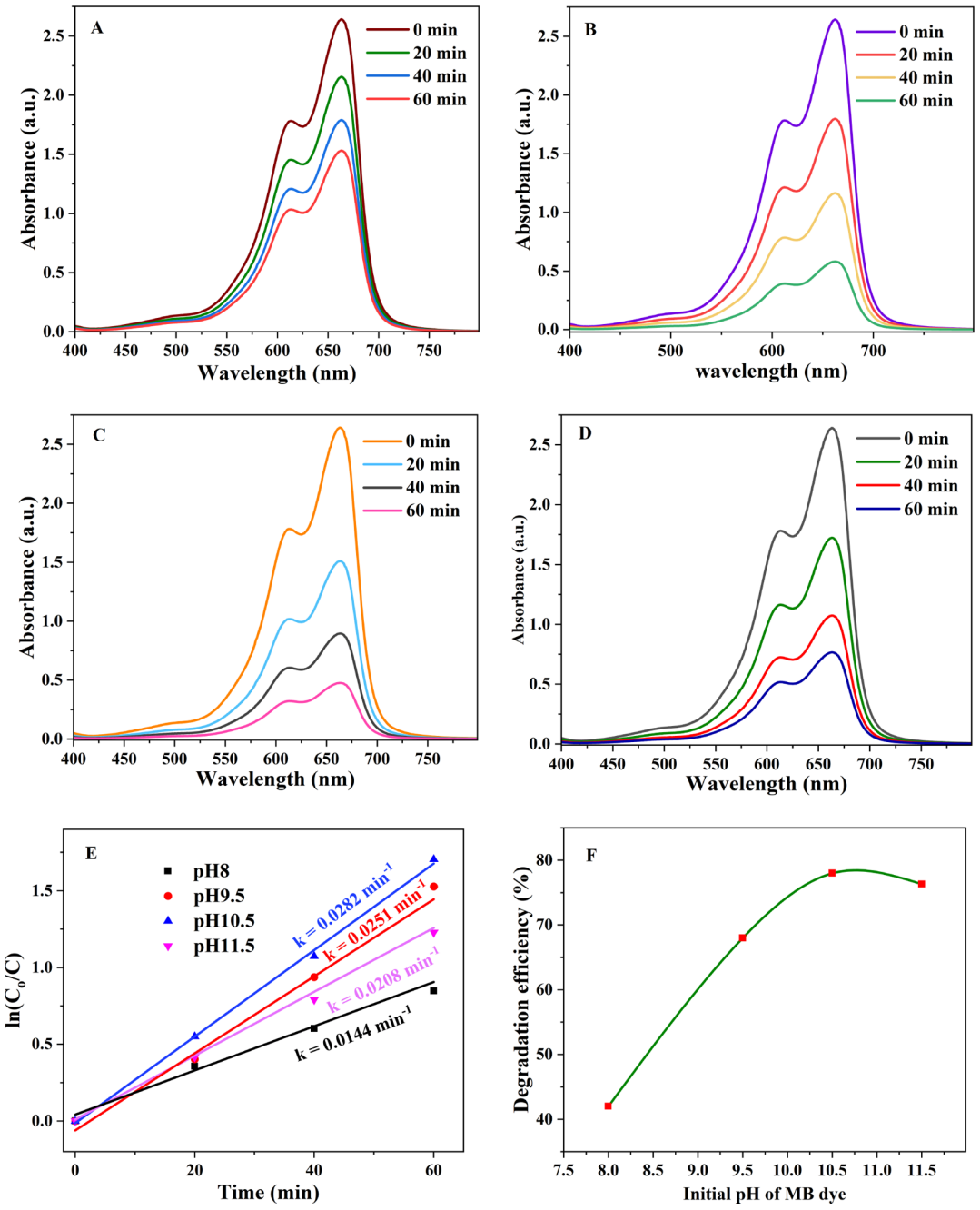

Figure 9. UV−vis absorption spectra of 15 ppm of MB dye with a catalyst dose of 30 mg at pH values of (A) 8, (B) 9.5, (C) 10.5, and (D) 11.5; (E) pseudo-first order model plot of (A−D); (F) degradation efficiency of (A−D).

($OH^{\bullet}$) were the dominant reactive species as the addition of IPA resulted in a decrease of degradation efficiency approximately to 38 (from 98% without a scavenger). Upon the addition of acetonitrile, the degradation efficiency decreased to 47%, which indicates that superoxide radicals ($O_2^{-\bullet}$) played a role in photodegradation of MB. The decrement of degradation efficiency to 54% as a result of addition of holes scavenger (EDTA-2Na) revealed good participation of holes (h^+) in the degradation mechanism. In general, the results appear to confirm the photocatalytic activity of IL-TiO_2,against MB dye driven by the reactive species in a sequence of $OH^{\bullet} > O_2^{\bullet-} > h^+ > e^-$, and similar results were reported by Saharudin et al.[76]

3.8. Mechanism of Photocatalysis. Upon irradiation of light energy that exceeds the band gap of IL-TiO_2, the electrons excite to the conduction band leaving holes in the valence band as shown in Figure 12 and given by eq 6.[77] The electrons generated in the conduction band of IL-TiO_2 are captured by O_2 adsorbed on the surface of the photocatalyst to produce very reactive superoxide anion radicals (eq 7), contributing to both direct MB degradation and indirect MB removal through reactions with H_2O to generate hydroxyl free radicals. The positively charged holes in the valence band react with water molecules or hydroxyl anions, resulting in hydrogen cation ions (H^+) and hydroxyl radicals ($OH^{\bullet}$). Hydroxyl radicals, which are powerful oxidants, can react with organic pollutants and degrade them to environmentally harmless

https://doi.org/10.1021/acsomega.3c06142
ACS Omega 2023, 8, 43999−44012

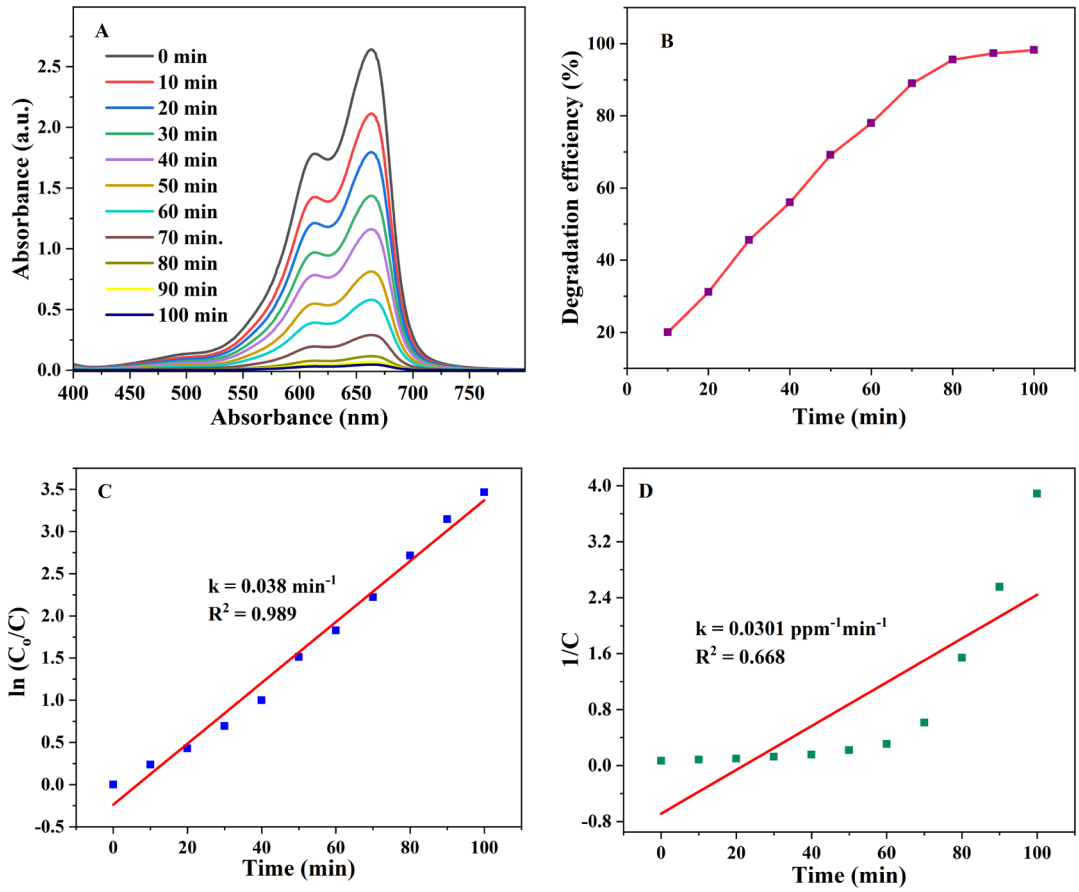

Figure 10. UV−vis absorption spectra of MB for 100 min at the optimized conditions (A); (B) degradation efficiency of (A); (C) pseudo-first order model plot of (A); (D) pseudo-second order model plot of (A).

Table 1. Comparison of the Photodegradation Efficiency of IL-TiO_2 with Other Recently Reported Works

plant	photocatalyst	Dye	Catalyst dosage	time (minutes)	efficiency (%)	references
Acalypha indica	TiO_2	MB	50 mg	360	98.5	68
Commelina benghalensis	TiO_2	MB	30 mg	120	65	69
Cannabis sativa	TiO_2	MB	10 mg	80	98.2	36
Cestrum nocturnum	TiO_2	MB	8 mg	40	80	70
Ceaspina pulcherrima	TiO_2	MB	10 mg	40	86	71
Nervila aragona	TiO_2	MB	10 mg	40	75	71
Manihot esculante	TiO_2	MB	10 mg	40	56	71
Cochlospermum Gossypium	TiO_2	MB	15 mg	120	99	72
Citrus Limetta	TiO_2	MB	70 mg	80	90	73
Impatiens rothii Hook.*f.*	TiO_2	MB	30 mg	100	98	this work

Table 2. Summary of Degradation Efficiency under Optimized Conditions

IL-TiO_2 dosage	MB dye concentration	pH	time	fitted model	rate constant (k)	correlation constant (R^2)
30 mg	15 ppm	10.5	100 min	pseudo-first order	0.038 min^{-1}	0.989
				pseudo-second order	0.03 $ppm^{-1}min^{-1}$	0.668

products.[18] Generally, the following steps take place in photocatalysis of organic pollutants (1) absorption of photon energy and excitation of electron to the conduction band, (2) reduction, (3) oxidation, and (4) pollutant degradation as given in eqs 6−13.[5,78−80]

$$IL - TiO_2 + hv \rightarrow IL - TiO_2(h^+_{VB} + e^-_{CB}) \quad (6)$$

$$e^-_{CB} + O_2 \rightarrow O_2^{\bullet -}) \quad (7)$$

$$O_2^{\bullet -} + H^+ \rightarrow HO_2^{\bullet} \quad (8)$$

$$2HO_2^{\bullet} \rightarrow H_2O_2 + O_2 \quad (9)$$

$$2HO_2^{\bullet} \rightarrow H_2O_2 + O_2^{\bullet -} \rightarrow OH^{\bullet} + O_2 + OH^- \quad (10)$$

$$h^+_{VB} + OH^- \rightarrow OH^{\bullet} \quad (11)$$

$$h^+_{VB} + H_2O \rightarrow OH^{\bullet} + H^+ \quad (12)$$

https://doi.org/10.1021/acsomega.3c06142
ACS Omega 2023, 8, 43999−44012

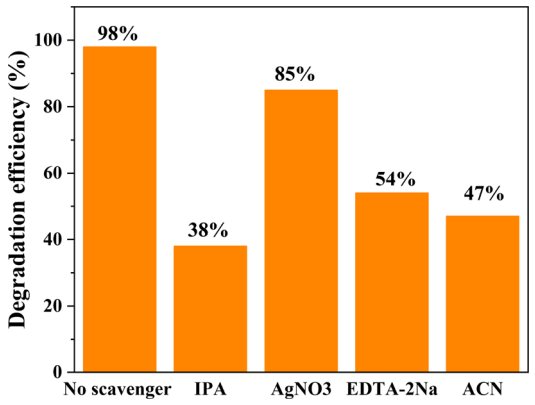

Figure 11. Effect of radical scavengers on the photodegradation ability of IL-TiO_2.

$$OH^{\bullet} + MB \rightarrow CO_2 + H_2O + \text{minerals} \quad (13)$$

3.9. Reusability Test. The photocatalyst recyclability and stability are key properties in cost minimization while maintaining durable and efficient photocatalytic performances in pollutants removal. The reusability test of IL−TiO_2 NPs showed good stability, and the percent removal values for the first, second, third, and fourth cycles were 96, 93.4, 91.7, and 88.3%, respectively, relative to the initial degradation efficiency (Figure 13).

4. CONCLUSIONS

In the present study, TiO_2 nanoparticles were effectively synthesized via a green synthetic method using *Impatiens rothii* Hook.*f* leaf extract as a reducing, capping, and stabilizing agent. Extensive evaluation of structural, thermal, optical, and crystallinity properties of the synthesized TiO_2 NPs has been performed using a number of characterization methods such as the Brunauer−Emmett−Teller (BET) analysis, high-resolution transmission electron microscopy (HRTEM), scanning electron microscopy(SEM), energy dispersive X-ray spectroscopy (EDX), Fourier transform infrared spectroscopy (FTIR), X-ray photoelectron spectroscopy (XPS), diffused reflectance spectroscopy (DRS), X-ray diffraction (XRD), and Raman spectroscopy. The specific surface area from BET analysis was found to be 65 m^2/g. The average crystallite size and particle size of synthesized NPs were found to be 11 and 25

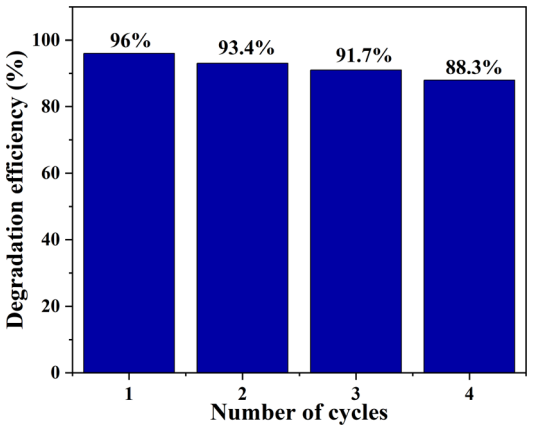

Figure 13. Recyclability test of IL−TiO_2 NPs for the photodegradation of MB dye.

nm, respectively. DRS analysis showed that the band gap of IL-TiO_2 was found to be 3.39 eV. The HRTEM micrograph showed the presence of grain boundary with *d* spacings of 0.352, 0.245, and 0.190, which correspond to the lattice planes of (101), (004), and (200), respectively. From the EDX analysis, weight percents of titanium and oxygen were found to be 54.33 and 45.67%, respectively, which confirms the presence of pure IL-TiO_2 nanoparticles. The synthesized NPs were found effective in the degradation of methylene blue in aqueous medium under a photocatalytic process. The removal efficiency of methylene blue under photocatalytic conditions was found to be 98% at the optimized parameters (initial MB dye concentration of 15 ppm, pH = 10.5, catalyst dosage of 30 mg, in the course of 100 min contact time). The kinetic analysis of photocatalytic degradation of MB showed that it was well fitted in a pseudo-first-order kinetic model with a correlation factor of 0.989. The reusability test showed good stability of IL−TiO_2 NPs.

■ ASSOCIATED CONTENT

Supporting Information

The Supporting Information is available free of charge at https://pubs.acs.org/doi/10.1021/acsomega.3c06142.

Experimental procedures for the preparation of plant extract and phytochemical analysis; (Figure S1) zero point charge determination of IL−TiO_2; (Figure S2)

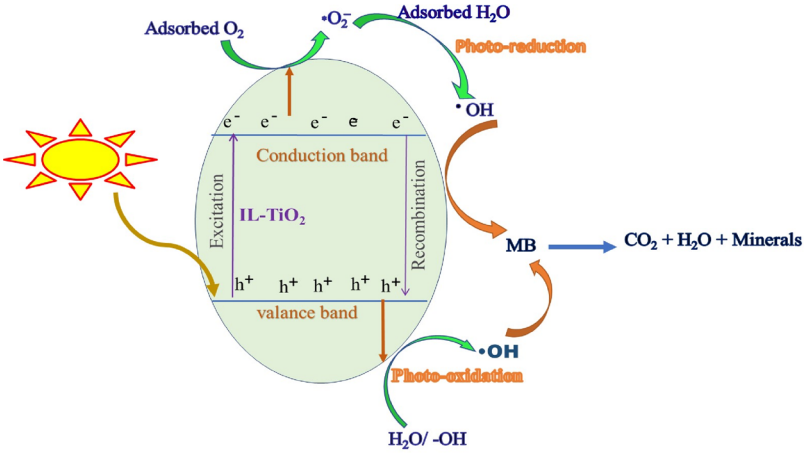

Figure 12. Proposed photodegradation mechanism of methylene blue by IL-TiO_2.

https://doi.org/10.1021/acsomega.3c06142
ACS Omega 2023, 8, 43999−44012

TGA-DTA for IL−TiO_2; (Figure S3) effect of IL−TiO_2 dose on photodegradation efficiency; (Figure S4) SEM image; (Figures S5−S7) photos of the solutions at different conditions; and (Table S1) phytochemical screening test summary (PDF)

AUTHOR INFORMATION

Corresponding Authors

Dereje Tsegaye Leku − *Department of Applied Chemistry, School of Applied and Natural Sciences, Adama Science and Technology University, Adama P.O. Box 1888, Ethiopia*; Email: detsegaye@gmail.com

Getachew Adam Workneh − *Department of Industrial Chemistry and Sustainable Energy Center of Excellence, Addis Ababa Science and Technology University, Addis Ababa P.O. Box 16417, Ethiopia*; orcid.org/0000-0002-2863-1379; Email: getachew.adam@aastu.edu.et

Author

Getye Behailu Yitagesu − *Department of Applied Chemistry, School of Applied and Natural Sciences, Adama Science and Technology University, Adama P.O. Box 1888, Ethiopia*

Complete contact information is available at: https://pubs.acs.org/10.1021/acsomega.3c06142

Author Contributions

Writing of the original draft and laboratory work was done by G.B. Writing of the review and editing of the paper was done by G.A. and D.T. All authors read the final revised manuscript in detail and approved it.

Notes

The authors declare no competing financial interest.

ACKNOWLEDGMENTS

The authors acknowledge Adama Science and Technology University, Ethiopia and Wachemo University, Ethiopia for their financial support.

REFERENCES

(1) Pavel, M.; Anastasescu, C.; State, R.-N.; Vasile, A.; Papa, F.; Balint, I. Photocatalytic degradation of organic and inorganic pollutants to harmless end products: assessment of practical application potential for water and air cleaning. *Catalysts* **2023**, *13* (2), 380.

(2) Al-Musawi, T. J.; Yilmaz, M.; Mohebi, S.; Balarak, D. Ultraviolet radiation/persulfate/hydrogen peroxide treatment system for the degradation of acid blue 80 dye from a batch flow chemical reactor: effects of operational parameters, mineralization, energy consumption, and kinetic studies. *Energy, Ecology and Environment* **2022**, *7* (6), 630−640.

(3) Crini, G.; Lichtfouse, E. Advantages and disadvantages of techniques used for wastewater treatment. *Environmental Chemistry Letters* **2019**, *17*, 145−155.

(4) Ghazy, N. M.; Ghaith, E. A.; Abou El-Reash, Y.; Zaky, R. R.; Abou El-Maaty, W. M.; Awad, F. S. Enhanced performance of hydroxyl and cyano group functionalized graphitic carbon nitride for efficient removal of crystal violet and methylene blue from wastewater. *RSC Adv.* **2022**, *12* (55), 35587−35597.

(5) Salem, B. B.; Essalah, G.; Ameur, S. B.; Duponchel, B.; Guermazi, H.; Guermazi, S.; Leroy, G. Synthesis and comparative study of the structural and optical properties of binary ZnO-based composites for environmental applications. *RSC Adv.* **2023**, *13* (9), 6287−6303.

(6) Dagar, S.; Singh, S. K.; Gupta, M. K. Economics of advanced technologies for wastewater treatment: Evidence from pulp and paper industry. *Frontiers in Environmental Science* **2022**, *10*, 960639.

(7) Abdel-Raouf, M. E.; Maysour, N. E.; Farag, R. K.; Abdul-Raheim, M. A. R. Wastewater treatment methodologies, review article. *Int. J. Environ. Agric. Sci.* **2019**, *3*, 018.

(8) Salama, R. S.; El-Sayed, E.-S. M.; El-Bahy, S. M.; Awad, F. S. Silver nanoparticles supported on UiO-66 (Zr): as an efficient and recyclable heterogeneous catalyst and efficient adsorbent for removal of Indigo Carmine. *Colloids Surf., A* **2021**, *626*, 127089.

(9) Sillanpää, M.; Mahvi, A. H.; Balarak, D.; Khatibi, A. D. Adsorption of Acid orange 7 dyes from aqueous solution using Polypyrrole/nanosilica composite: Experimental and modelling. *International Journal of Environmental Analytical Chemistry* **2023**, *103* (1), 212−229.

(10) Rezaei, M.; Mengelizadeh, N.; Berizi, Z.; Salehnia, S.; Asgari, M.; Balarak, D. Synthesis of MMT− CuFe2O4 Composite as a Peroxymonosulfate Activator for the Degradation of Reactive Black 5. *ChemistrySelect* **2023**, *8* (2), e202201729.

(11) Bakry, A. M.; Alamier, W. M.; El-Shall, M. S.; Awad, F. S. Facile synthesis of amorphous zirconium phosphate graphitic carbon nitride composite and its high performance for photocatalytic degradation of indigo carmine dye in water. *Journal of Materials Research and Technology* **2022**, *20*, 1456−1469.

(12) Landi, S., Jr; Segundo, I. R.; Freitas, E.; Vasilevskiy, M.; Carneiro, J.; Tavares, C. J. Use and misuse of the Kubelka-Munk function to obtain the band gap energy from diffuse reflectance measurements. *Solid state communications* **2022**, *341*, 114573.

(13) Zhu, S.; Wang, D. Photocatalysis: basic principles, diverse forms of implementations and emerging scientific opportunities. *Adv. Energy Mater.* **2017**, *7* (23), 1700841.

(14) Yilmaz, M.; Mengelizadeh, N.; Saloot, M. k.; shahbaksh, S.; Balarak, D. Facile synthesis of Fe3O4/ZnO/GO photocatalysts for decolorization of acid blue 113 under solar, visible and UV lights. *Mater. Sci. Semicond. Process.* **2022**, *144*, 106593.

(15) Chelliah, P.; Wabaidur, S. M.; Sharma, H. P.; Majdi, H. S.; Smait, D. A.; Najm, M. A.; Iqbal, A.; Lai, W.-C. Photocatalytic Organic Contaminant Degradation of Green Synthesized ZrO2 NPs and Their Antibacterial Activities. *Separations* **2023**, *10* (3), 156.

(16) Vinothkanna, A.; Mathivanan, K.; Ananth, S.; Ma, Y.; Sekar, S. Biosynthesis of copper oxide nanoparticles using Rubia cordifolia bark extract: characterization, antibacterial, antioxidant, larvicidal and photocatalytic activities. *Environmental Science and Pollution Research* **2023**, *30* (15), 42563−42574.

(17) Abbaspoor, M.; Aliannezhadi, M.; Tehrani, F. S. High-performance photocatalytic WO3 nanoparticles for treatment of acidic wastewater. *J. Sol-Gel Sci. Technol.* **2023**, *105* (2), 565−576.

(18) K K, S.; P M, P. N.; Vasundhara, M. Enhanced photocatalytic activity in ZnO nanoparticles developed using novel Lepidagathis ananthapuramensis leaf extract. *RSC Adv.* **2023**, *13* (3), 1497−1515.

(19) Abbood, H. K.; Ali, N. A. Studying of the structural and optical properties of titanium dioxide nanoparticles prepared by chemical method *J. Opt.* **2023** 1 6 DOI: .

(20) Danish, M. S. S.; Estrella, L. L.; Alemaida, I. M. A.; Lisin, A.; Moiseev, N.; Ahmadi, M.; Nazari, M.; Wali, M.; Zaheb, H.; Senjyu, T. Photocatalytic applications of metal oxides for sustainable environmental remediation. *Metals* **2021**, *11* (1), 80.

(21) Ali, I.; Suhail, M.; Alothman, Z. A.; Alwarthan, A. Recent advances in syntheses, properties and applications of TiO 2 nanostructures. *RSC Adv.* **2018**, *8* (53), 30125−30147.

(22) Sagadevan, S.; Imteyaz, S.; Murugan, B.; Anita Lett, J.; Sridewi, N.; Weldegebrieal, G. K.; Fatimah, I.; Oh, W.-C. A comprehensive review on green synthesis of titanium dioxide nanoparticles and their diverse biomedical applications. *Green Processing and Synthesis* **2022**, *11* (1), 44−63.

(23) Luthfiah, A.; Permana, M. D.; Deawati, Y.; Firdaus, M. L.; Rahayu, I.; Eddy, D. R. Photocatalysis of nanocomposite titania−natural silica as antibacterial against Staphylococcus aureus and Pseudomonas aeruginosa. *RSC Adv.* **2021**, *11* (61), 38528−38536.

(24) Nyamukamba, P.; Okoh, O.; Mungondori, H.; Taziwa, R.; Zinya, S.; Yang, D. Synthetic methods for titanium dioxide nanoparticles: a review. *Titanium Dioxide-Mater. Sustainable Environ.* **2018**, *8*, 151−175.
(25) Waghmode, M. S.; Gunjal, A. B.; Mulla, J. A.; Patil, N. N.; Nawani, N. N. Studies on the titanium dioxide nanoparticles: Biosynthesis, applications and remediation. *SN Appli. Sci.* **2019**, *1* (4), 310.
(26) Nunes, D.; Fortunato, E.; Martins, R. Flexible nanostructured TiO2-based gas and UV sensors: A review. *Discover Mater.* **2022**, *2* (1), 2.
(27) Das, R.; Ambardekar, V.; Bandyopadhyay, P. P., Titanium dioxide and its applications in mechanical, electrical, optical, and biomedical fields. *Titanium Dioxide-Advances Applications* **2021**. DOI: 10.5772/intechopen.98805
(28) Wu, X., Applications of titanium dioxide materials. *Titanium Dioxide—Advances and Applications* **2022**. DOI: 10.5772/intechopen.99255
(29) Jayachithra, J.; Elampari, K.; Meena, M. Fabrication of TiO2 based Dye-Sensitized Solar Cell using Nerium oleander as a sensitizer. *OP Conf. Ser.: Mater. Sci. Eng. IOP Publishing* **2022**, *1263*, 012018 DOI: 10.1088/1757-899X/1263/1/012018.
(30) Arun, J.; Nachiappan, S.; Rangarajan, G.; Alagappan, R. P.; Gopinath, K.; Lichtfouse, E. Synthesis and application of titanium dioxide photocatalysis for energy, decontamination and viral disinfection: A review. *Environmental Chemistry Letters* **2023**, *21* (1), 339−362.
(31) Naldoni, A.; Altomare, M.; Zoppellaro, G.; Liu, N.; Kment, S.; Zboril, R.; Schmuki, P. Photocatalysis with reduced TiO2: from black TiO2 to cocatalyst-free hydrogen production. *ACS catalysis* **2019**, *9* (1), 345−364.
(32) Bonkerud, J.; Zimmermann, C.; Weiser, P. M.; Vines, L.; Monakhov, E. V., On the dielectric constant of titanium dioxide. 2021 DOI: 10.21203/rs.3.rs-301495/v1.
(33) Rehman, Z. U.; Bilal, M.; Hou, J.; Butt, F. K.; Ahmad, J.; Ali, S.; Hussain, A. Photocatalytic CO2 reduction using TiO2-based photocatalysts and TiO2 z-scheme heterojunction composites: A review. *Molecules* **2022**, *27* (7), 2069.
(34) Bekru, A. G.; Tufa, L. T.; Zelekew, O. A.; Goddati, M.; Lee, J.; Sabir, F. K. Green Synthesis of a CuO−ZnO Nanocomposite for Efficient Photodegradation of Methylene Blue and Reduction of 4-Nitrophenol. *ACS omega* **2022**, *7* (35), 30908−30919.
(35) Feinle, A.; Hüsing, N. Liquid-Phase Synthesis of Metal Oxide Nanoparticles. *Metal Oxide Nanoparticles: Formation, Functional Properties, and Interfaces* **2021**, *1*, 109−150.
(36) BinSabt, M.; Sagar, V.; Singh, J.; Rawat, M.; Shaban, M. Green synthesis of CS-TiO2 NPs for efficient photocatalytic degradation of methylene blue dye. *Polymers* **2022**, *14* (13), 2677.
(37) Srinivasan, M.; Venkatesan, M.; Arumugam, V.; Natesan, G.; Saravanan, N.; Murugesan, S.; Ramachandran, S.; Ayyasamy, R.; Pugazhendhi, A. Green synthesis and characterization of titanium dioxide nanoparticles (TiO2 NPs) using Sesbania grandiflora and evaluation of toxicity in zebrafish embryos. *Process Biochemistry* **2019**, *80*, 197−202.
(38) Narayanan, M.; Devi, P. G.; Natarajan, D.; Kandasamy, S.; Devarayan, K.; Alsehli, M.; Elfasakhany, A.; Pugazhendhi, A. Green synthesis and characterization of titanium dioxide nanoparticles using leaf extract of Pouteria campechiana and larvicidal and pupicidal activity on Aedes aegypti. *Environmental Research* **2021**, *200*, 111333.
(39) Yohannis, S. W.; Asfaw, Z.; Kelbessa, E. Ethnobotanical study of medicinal plants used by local people in menz gera midir district, north shewa zone, amhara regional state, Ethiopia. *J. Med. Plants Res.* **2018**, *12* (21), 296−314.
(40) Basit, R. A.; Abbasi, Z.; Hafeez, M.; Ahmad, P.; Khan, J.; Khandaker, M. U.; Al-Mugren, K. S.; Khalid, A. Successive photocatalytic degradation of methylene blue by ZnO, CuO and ZnO/CuO synthesized from coriandrum sativum plant extract via green synthesis technique. *Crystals* **2023**, *13* (2), 281.
(41) Al-Maliky, E. A.; Gzar, H. A.; Al-Azawy, M. G. Determination of point of zero charge (PZC) of concrete particles adsorbents. *IOP Conf. Ser.: Mater. Sci. Eng. IOP Publishing* **2021**, *1184*, 012004 DOI: 10.1088/1757-899X/1184/1/012004.
(42) Akerdi, A. G.; Bahrami, S. H.; Pajootan, E. Modeling and optimization of Photocatalytic Decolorization of binary dye solution using graphite electrode modified with Graphene oxide and TiO 2. *Journal of Environmental Health Science and Engineering* **2020**, *18*, 51−62.
(43) Guo, X.; Wang, X.; Niu, Y. Visible Light Driven Photocatalytic Degradation of Norfloxacin Using 3D Supramolecular Compounds. *J. Cluster Sci.* **2023**, *34*, 2643−2652.
(44) Zhu, X.; Han, S.; Feng, W.; Kong, Q.; Dong, Z.; Wang, C.; Lei, J.; Yi, Q. The effect of heat treatment on the anatase−rutile phase transformation and photocatalytic activity of Sn-doped TiO 2 nanomaterials. *RSC Adv.* **2018**, *8* (26), 14249−14257.
(45) Shimi, A. K.; Ahmed, H. M.; Wahab, M.; Katheria, S.; Wabaidur, S. M.; Eldesoky, G. E.; Islam, M. A.; Rane, K. P. Synthesis and applications of green synthesized TiO_2 nanoparticles for photocatalytic dye degradation and antibacterial activity. *J. Nanomater.* **2022**, *2022*, 7060388 DOI: 10.1155/2022/7060388.
(46) Abebe, B. Synergetic and charge transfer properties of a metal oxide heterojunction: Photocatalytic activities. *Frontiers in Catalysis* **2022**, *2*, 950384.
(47) Toncón-Leal, C. F.; Villarroel-Rocha, J.; Silva, M. T. P. d.; Braga, T. P.; Sapag, K. Characterization of mesoporous region by the scanning of the hysteresis loop in adsorption−desorption isotherms. *Adsorption* **2021**, *27* (7), 1109−1122.
(48) Baudys, M.; Berthet, E.; Macak, J. M.; Lhotka, M.; Krýsa, J. Photocatalytic degradation of gaseous pollutants on nanostructured TiO2 films of various thickness and surface area. *Photochem. Photobiol. Sci.* **2023**, *22*, 883−892.
(49) Bharti, B.; Kumar, S.; Lee, H.-N.; Kumar, R. Formation of oxygen vacancies and Ti3+ state in TiO2 thin film and enhanced optical properties by air plasma treatment. *Sci. Rep.* **2016**, *6* (1), 32355.
(50) Azeez, F.; Al-Hetlani, E.; Arafa, M.; Abdelmonem, Y.; Nazeer, A. A.; Amin, M. O.; Madkour, M. The effect of surface charge on photocatalytic degradation of methylene blue dye using chargeable titania nanoparticles. *Sci. Rep.* **2018**, *8* (1), 7104.
(51) Matouk, Z.; Islam, M.; Gutiérrez, M.; Pireaux, J.-J.; Achour, A. X-ray Photoelectron Spectroscopy (XPS) Analysis of Ultrafine Au Nanoparticles Supported over Reactively Sputtered TiO2 Films. *Nanomaterials* **2022**, *12* (20), 3692.
(52) Nandiyanto, A. B. D.; Oktiani, R.; Ragadhita, R. How to read and interpret FTIR spectroscope of organic material. *Indonesian Journal of Science and Technology* **2019**, *4* (1), 97−118.
(53) Alamier, W. M.; DY Oteef, M.; Bakry, A. M.; Hasan, N.; Ismail, K. S.; Awad, F. S. Green Synthesis of Silver Nanoparticles Using Acacia ehrenbergiana Plant Cortex Extract for Efficient Removal of Rhodamine B Cationic Dye from Wastewater and the Evaluation of Antimicrobial Activity. *ACS Omega* **2023**, *8*, 18901 DOI: 10.1021/acsomega.3c01292.
(54) Mansour, S. A.; Farha, A.; Kotkata, M. Sol−Gel Synthesized Co-Doped Anatase TiO 2 Nanoparticles: Structural, Optical, and Magnetic Characterization. *Journal of Inorganic and Organometallic Polymers and Materials* **2019**, *29*, 1375−1382.
(55) Aravind, M.; Amalanathan, M.; Mary, M. S. M. Synthesis of TiO 2 nanoparticles by chemical and green synthesis methods and their multifaceted properties. *SN Appl. Sci.* **2021**, *3*, 1−10.
(56) Ali, H. M.; Ibrahim, S. M.; Zeid, E. F. A.; Al-Hossainy, A. F.; Abd El-Aal, M. A comparative study of Cu-anchored 0D and 1D ZnO nanostructures for the reduction of organic pollutants in water. *RSC Adv.* **2022**, *12* (26), 16496−16509.
(57) Liao, D.; Zhi, J.; Wang, Q.; Yan, W.; Guo, Y.; Han, Y.; Dong, C.; Xiao, Y.; Bai, H.; Liang, W.; Fan, L. Efficient photoelectrochemical aptasensing of di-2-ethylhexyl phthalate in environmental samples based on N, S co-doped graphene quantum dots/TiO2 nanorods.

Anal. Chim. Acta **2023**, *1271*, 341477 DOI: 10.1016/j.aca.2023.341477.
(58) Farooq, U.; Ahmed, J.; Alshehri, S. M.; Ahmad, T. High-surface-area sodium tantalate nanoparticles with enhanced photocatalytic and electrical properties prepared through polymeric citrate precursor route. *ACS omega* **2019**, *4* (21), 19408−19419.
(59) Wypych, A.; Bobowska, I.; Tracz, M.; Opasinska, A.; Kadlubowski, S.; Krzywania-Kaliszewska, A.; Grobelny, J.; Wojciechowski, P. Dielectric properties and characterisation of titanium dioxide obtained by different chemistry methods. *J. Nanomater.* **2014**, *2014*, 1−9.
(60) El-Deen, S.; Hashem, A.; Abdel Ghany, A.; Indris, S.; Ehrenberg, H.; Mauger, A.; Julien, C. Anatase TiO 2 nanoparticles for lithium-ion batteries. *Ionics* **2018**, *24*, 2925−2934.
(61) Raguram, T.; Rajni, K. Synthesis and analysing the structural, optical, morphological, photocatalytic and magnetic properties of TiO 2 and doped (Ni and Cu) TiO 2 nanoparticles by sol−gel technique. *Appl. Phys. A: Mater. Sci. Process.* **2019**, *125*, 1−11.
(62) Kundu, A.; Mondal, A. Photodegradation of methylene blue under direct sunbeams by synthesized anatase titania nanoparticles. *SN Appl. Sci.* **2019**, *1*, 1−17.
(63) Al-Taweel, S. S.; Saud, H. R. New route for synthesis of pure anatase TiO2 nanoparticles via utrasound-assisted sol-gel method. *J. Chem. Pharm. Res.* **2016**, *8* (2), 620−626.
(64) Makuła, P.; Pacia, M.; Macyk, W. How to correctly determine the band gap energy of modified semiconductor photocatalysts based on UV−Vis spectra. *ACS Publications* **2018**, *9*, 6814−6817.
(65) Praveen, P.; Viruthagiri, G.; Mugundan, S.; Shanmugam, N. Structural, optical and morphological analyses of pristine titanium dioxide nanoparticles−Synthesized via sol−gel route. *Spectrochimica Acta Part A: Molecular and Biomolecular Spectroscopy* **2014**, *117*, 622−629.
(66) Mortazavian, S.; Saber, A.; James, D. E. Optimization of photocatalytic degradation of acid blue 113 and acid red 88 textile dyes in a UV-C/TiO2 suspension system: application of response surface methodology (RSM). *Catalysts* **2019**, *9* (4), 360.
(67) Reza, K. M.; Kurny, A.; Gulshan, F. Parameters affecting the photocatalytic degradation of dyes using TiO 2: a review. *Applied Water Science* **2017**, *7*, 1569−1578.
(68) Rao, K. G.; Ashok, C.; Rao, K. V.; Chakra, C.; Tambur, P. Green synthesis of TiO2 nanoparticles using Aloe vera extract. *Int. J. Adv. Res. Phys. Sci.* **2015**, *2* (1A), 28−34.
(69) Bopape, D. A.; Tetana, Z. N.; Mabuba, N.; Motaung, D. E.; Hintsho-Mbita, N. C. Biosynthesis of TiO2 nanoparticles using Commelina benghanlensis for the photodegradation of methylene blue dye and antibiotics: effect of plant concentration. *Results in Chemistry* **2023**, *5*, 100825.
(70) Amanulla, A. M.; Sundaram, R. Green synthesis of TiO2 nanoparticles using orange peel extract for antibacterial, cytotoxicity and humidity sensor applications. *Mater. Today: Proc.* **2019**, *8*, 323−331.
(71) Rathi, V. H.; Jeice, A. R. Green fabrication of titanium dioxide nanoparticles and their applications in photocatalytic dye degradation and microbial activities. *Chemical Physics Impact* **2023**, *6*, 100197.
(72) Saranya, K. S.; Vellora Thekkae Padil, V.; Senan, C.; Pilankatta, R.; Saranya, K.; George, B.; Wacławek, S.; Černík, M. Green synthesis of high temperature stable anatase titanium dioxide nanoparticles using gum kondagogu: characterization and solar driven photocatalytic degradation of organic dye. *Nanomaterials* **2018**, *8* (12), 1002.
(73) Nabi, G.; Majid, A.; Riaz, A.; Alharbi, T.; Kamran, M. A.; Al-Habardi, M. Green synthesis of spherical TiO2 nanoparticles using Citrus Limetta extract: Excellent photocatalytic water decontamination agent for RhB dye. *Inorg. Chem. Commun.* **2021**, *129*, 108618.
(74) Mugumo, R.; Ichipi, E.; Tichapondwa, S. M.; Chirwa, E. M. N., Visible-Light-Induced Photocatalytic Degradation of Rhodamine B Dye Using CuS/ZnS PN Heterojunction Nanocomposite under Visible Light Irradiation. 2023 DOI: 10.20944/preprints202306.1272.v1.
(75) Salesi, S.; Nezamzadeh-Ejhieh, A. An experimental design study of photocatalytic activity of the Z-scheme silver iodide/tungstate binary nano photocatalyst. *Environ. Sci. Pollut. Res.* **2023**, *30*, 105440−105456.
(76) Saharudin, K. A.; Sreekantan, S.; Basiron, N.; Khor, Y. L.; Harun, N. H.; Mydin, R. B. S. M. N.; Md Akil, H.; Seeni, A.; Vignesh, K. Bacteriostatic Activity of LLDPE Nanocomposite Embedded with Sol−Gel Synthesized TiO2/ZnO Coupled Oxides at Various Ratios. *Polymers* **2018**, *10* (8), 878.
(77) Zhang, Y.; Miao, B.; Chen, Q.; Bai, Z.; Cao, Y.; Davaa, B. Synthesis, structure, and photocatalytic activity of TiO2-montmorillonite composites. *Catalysts* **2022**, *12* (5), 486.
(78) Kumari, H.; Sonia; Suman; Ranga, R.; Chahal, S.; Devi, S.; Sharma, S.; Kumar, S.; Kumar, P.; Kumar, S.; Kumar, A.; Parmar, R. A Review on Photocatalysis Used For Wastewater Treatment: Dye Degradation. *Water, Air, Soil Pollut.* **2023**, *234* (6), 349.
(79) Tahir, M. B.; Sohaib, M.; Sagir, M.; Rafique, M. Role of nanotechnology in photocatalysis. *Encyclopedia of Smart Materials* **2022**, 578.
(80) Kermani, M.; Mostafapour, A.; Sabouri, Z.; Gheibihayat, S. M.; Darroudi, M. The photocatalytic, cytotoxicity, and antibacterial properties of zinc oxide nanoparticles synthesized using Trigonella foenum-graecum L extract. *Environmental Science and Pollution Research* **2023**, *30* (7), 19313−19325.

https://doi.org/10.1021/acsomega.3c06142
ACS Omega 2023, 8, 43999−44012